Journal of ELECTRONIC MATERIALS, Vol. 50, No. 5, 2021
https://doi.org/10.1007/s11664-020-08729-z

ORIGINAL RESEARCH ARTICLE

Facile Synthesis of $CeO_2/CoWO_4$ Hybrid Nanocomposites for High Photocatalytic Performance and Investigation of Antimicrobial Activity

S. SELVI,[1] RANJITH RAJENDRAN,[2] D. BARATHI,[3] and N. JAYAMANI[1,4]

1.—Department of Physics, Government Arts College (Autonomous), Salem, Tamil Nadu 636007, India. 2.—Department of Physics, Periyar University, Salem, Tamil Nadu 636 011, India. 3.—Department of Physics, N.K.R Government Arts College, Namakkal, Tamil Nadu 637001, India. 4.—e-mail: jayamaniphysics@gmail.com

In this work, novel $CeO_2/CoWO_4$ heterostructured nanocomposites (NCs) were synthesized via a hydrothermal method. X-ray diffraction, high-resolution transmission electron microscopy, UV–Vis diffuse reflectance spectroscopy and photoluminescence spectroscopy were carried out to determine the crystal structure, deep morphology, optical properties, and charge separation of the obtained photocatalysts (PCs), respectively. In comparison to the pristine $CoWO_4$, the CeO_2 and $CeO_2/CoWO_4$ PCs demonstrated enhanced activity of methylene blue (MB) aqueous dye photodegradation under visible-light exposure. The photodegradation efficiency of the as-prepared $CeO_2/CoWO_4$ photocatalyst showed the premier decomposition ratio (92.5%) of MB dye in 105 min among all samples, which was notably 1.8-fold and 2.2-fold that of the pristine CeO_2 (43%) and $CoWO_4$ (60%), respectively. Likewise, the $CeO_2/CoWO_4$ PCs retained satisfactory photo-reactivity even after five sequential recycling runs, indicating their excellent photocatalytic stability and robustness. Hence the succeeding superior PCs preferred further efficient charge (e^-–h^+) separation, excellent visible-light absorption, and worthy interfacial energy transfer leads between $CoWO_4$ and CeO_2 nanoparticles. Additionally, a plausible mechanism for the photodegradation was proposed. The synergistic antibacterial properties of the $CeO_2/CoWO_4$ NCs were investigated by a gel diffusion method. Therefore, this work offers a novel avenue for the preparation of stable and efficient visible-light-driven PCs for environmental remediation.

Key words: $CeO_2/CoWO_4$ nanocomposites, visible light, photodegradation, methylene blue dye, recyclability

INTRODUCTION

Photocatalysis is considered one of the most effective ways to resolve the growing environmental weakening fuel and energy problems. Semiconductor (SC)-based photocatalysts (PCs) have attracted much attention in several multidisciplinary fields including materials, environment, and chemistry, and are highly favored for the elimination of hazardous toxins in polluted water.[1,2] It has been widely acknowledged that environmental pollution as a result of rapid industrialization and population growth is one of the most serious issues facing society globally. However, none of these semiconductor PCs can certainly fulfill for entire provisions of real uses, for existence in the excessive exploitation of solar energy, great effectiveness, high stability and low cost.[3,4] For instance, one of the most important and low-cost dyes, methylene blue (MB), is commonly used for textile dyeing, photography

(Received September 24, 2020; accepted December 24, 2020; published online March 6, 2021)

and printing trades, and retains its carcinogenic and mutagenic effects in wildlife, chronic noxiousness and can even bio-accumulate in the food chain towards humans and animals.[4,5] Accordingly, the elimination of MB dye from wastewater by visible-light-driven (VLD) photocatalytic processes represents a feasible and environmentally friendly approach to exploit solar energy in order to reduce environmental pollutants.[6] The photocatalytic activity of transition metal oxides (TMO) and lanthanides has recently received much attention in studies investigating the photodegradation of organic toxins in aqueous solutions under UV or visible-light treatment.[7]

Among several lanthanides, CeO_2 nanostructured (NS) materials have garnered considerable interest over the past decade because of their distinctive properties, with extensive application in catalysis, gas sensors, antibacterial agents,[8] ultraviolet ray detectors, and eco-friendly dyes.[9,10] CeO_2 is a chemically stable oxide nanomaterial, with an array of unique properties including excellent optical transparency in the visible region, stability at high temperatures, robustness and ability of provided that oxygen species to easy source or relief oxygen alteration between Ce^{3+} and Ce^{4+} oxidation states of their lattice oxygen assembly in oxygen vacancies (V_o). Cobalt tungstate ($CoWO_4$), as a unique transition metal tungstate photocatalyst, has a narrow-bandgap as a *p*-type semiconductor ($E_g = \sim 2.8$ eV). Because of its great stability, environmentally friendly nature and low-cost preparation,[11] $CoWO_4$ has been used in sensors, dye essences, supercapacitors, photovoltaic electrochemical cells, and photocatalyst decomposition.[12] However, owing to the short efficiency of (e^-–h^+) separation, the photocatalytic activity of pristine $CoWO_4$ nanomaterials (NMs) is quite low. As is well-recognized by researchers, the combination of SCs can significantly improve the photocatalytic activity of pristine NMs by enhancing their charge separation capability and increasing their light-trapping activity.[12,13] Thus, emerging owing PCs by enhancing properties over the pairing, co-catalysts accumulation, fashioning right heterojunction and further serious one. It has instantly preferred to progress the proficient VLD photocatalyst by moderately great charge-separation efficacy, also generate photo-carrier traps and reduce electron–hole (e^-–h^+) pair recombination. To the best of our knowledge, no studies have been reported on the combination of CeO_2/$CoWO_4$ PCs and the subsequent application for dye removal in environmental remediation. Hence, the preparation of CeO_2 blended in $CoWO_4$ to form $CeO_2/CoWO_4$ NCs was likely to attain high performance as a photocatalyst for aqueous-phase MB dye removal under visible light. Later, too overwhelmed the forbidden bandwidth, relaxed recombination of (e^-–h^+) pairs and small consumption of solar energy to a certain extent, whereas it could captivate better visible light range, greater catalytic activity and stable performance.[14]

In the current study, the successful preparation of novel $CeO_2/CoWO_4$ NCs via hydrothermal surface chemistry is described. These hybrid systems achieved excellent reproducibility and facilitated the generation of high-purity yields. The as-prepared PCs demonstrated significantly enhanced photodegradation of MB dye. The structural, morphological and optical properties of the CeO_2/$CoWO_4$ PCs were further characterized to investigate the underlying mechanism. The distinct improvement in photocatalytic activity benefited from the electron (e^-) transfer from $CoWO_4$ into CeO_2 controlled by visible-light frequency. The rapid electron (e^-) promotion from $CoWO_4$ into CeO_2 resulted in both a lower recombination rate and longer lifetime of the photoexcited charges. Therefore, this novel $CeO_2/CoWO_4$ NC method enables more effective solar energy exploitation of the photo-excited (e^-) in CeO_2 with an enhanced photocatalytic performance and antibacterial performance.

EXPERIMENTAL SECTION

Materials

For this study, cobalt nitrate hexahydrate ($Co(NO_3)_3{\cdot}6H_2O$; 99%), sodium tungstate dihydrate ($Na_2WO_4{\cdot}2H_2O$, 99%), and ethylene glycol (99%) were procured from Himedia Ltd. Potassium chloride (Merck, 99%) and cerium nitrate ($Ce(NO_3)_3{\cdot}6H_2O$; 98%) were obtained from SRL Chem. Limited. Sodium hydroxide (NaOH), isopropanol (IPA), ethylenediaminetetraacetic acid disodium salt (EDTA-2Na), benzoquinone (BQ), and absolute ethanol (CH_3CH_2OH) were obtained from SDFCL Chemical Reagent Co., Pvt. Ltd. Methylene blue (MB; $C_{16}H_{18}ClN_3S$) dye was obtained from SD Fine and was used as received. All the chemicals were of analytical/methodical reagent (AR) grade and were used without further purification. Deionized (DI) water was used in all experiments.

Preparation of $CeO_2/CoWO_4$ Nanomaterials

Briefly, 0.03 mol of $Ce(NO_3)_3{\cdot}6H_2O$ was ultrasonically dissolved in 100 mL of DI water. NH_4OH was added dropwise to the above solution to reach pH ~ 12. Lastly, the composed precipitates[9] were dried at 60°C for 8 h and further calcined at 400°C for 1.5 h to obtain CeO_2 NMs. In this research, the CeO_2 was mixed with $CoWO_4$ NMs, and then 0.03 mol of $Co(NO_3)_3{\cdot}6H_2O$ and 0.03 mol of $Na_2WO_4.2H_2O$ solution were added by 50 mL of DI water. Next, 1 mol (50 mL) of NH_4OH solution was added to the pioneer solution, although the pH value reached ~ 11–12. After stirring for 3 h, 0.1 g of the as-obtained CeO_2 NMs was also added to the above solution and then stirred for 2 h. The reaction mixture was then transferred to a 250 mL Teflon-

lined stainless steel autoclave and heated at 160°C for 24 h. Finally, the $CeO_2/CoWO_4$ precipitate was obtained via centrifugation, followed by thorough washing with DI water and ethanol, and drying at 65°C for 8 h. The $CeO_2/CoWO_4$ NCs were similarly obtained.[15] Following this scheme, the pristine $CoWO_4$ NPs were obtained by a similar process but without accumulation of CeO_2 NMs.

Characterization of the As-Prepared Samples

The x-ray diffraction (XRD) patterns were acquired on an x-ray diffractometer (Rigaku Mini-Flex II; x-ray diffractometer) with CuKα radiation. FTIR analysis was performed using a PerkinElmer RX1 FTIR spectrophotometer. The surface morphologies of the as-prepared NMs were investigated via high-resolution scanning electron microscopy (HR-SEM; HITACHI S-3000 H). The deep morphology, shape and particle size of the sample were recorded by high-resolution transmission electron microscopy (HR-TEM) images using JEM-2011 instrument (JEOL, Japan). The optical properties of the obtained samples were assessed using a UV–Vis DRS spectrophotometer (UV2550, Shimadzu, Japan). The optical absorption of dye degradation in the samples was measured via a UV–Vis spectrophotometer (PerkinElmer Lambda 19). The photoelectron transfer of the catalyst was studied by photoluminescence (PL) spectroscopy using a PerkinElmer LS-45 spectrometer at an excitation wavelength of $\sim$ 321 nm.

Photocatalytic Activity of MB dye Degradation

The photodegradation performance of the as-obtained samples (50 mg) was measured by the degradation of MB dye (20 ppm; 100 mL solution; 10 mg/L) under visible-light exposure (300 W Xe lamp by $\lambda >$ 420 nm cutoff filter in a Pyrex photocatalytic vessel).[16] Prior to exposure, the suspension was subjected to constant magnetic stirring for around 30 min in the dark to confirm that the dyes might extend the absorption-desorption equilibrium on the photocatalyst surface and dyes.[17] At specific intervals, 2.5 mL of the suspension was extracted by centrifugation for 15 min of light irradiation, and the concentration of the composing solution was explored by gauging the concentrated absorbance of the MB dye in the peak at $\sim$ 664 nm. The photodegradation efficiency was expressed as the following formula: Efficiency (%) = $(C_0 - C_t)/C_0$*100, where C_0 and C_t are the UV–visible absorbance spectra rate of the dye solution before and after degradation. In order to detect the reactive species caused/trapping mechanism throughout the photocatalytic process, 1mM of IPA, BQ, and EDTA-2Na were added as quenchers of hydroxyl radicals ($^{\cdot}OH^{-}$), superoxide radical ($O_2^{\cdot -}$) and holes (h^+), respectively.[18]

Antibacterial Activity

The antibacterial activity of $CeO_2/CoWO_4$ NCs against gram-negative [*Escherichia coli* (*E. coli*)] and gram-positive [*Staphylococcus aureus* (*S. aureus*)] pathogenic bacterial strains was investigated using the agar gel diffusion method. The $CeO_2/CoWO_4$ NCs were dispersed in DMSO to a final concentration, and the solutions were filtered by Millipore filters for sterilization. The gel impregnated with 25 μg/mL, 50 μg/mL and 75 μg/mL of sample solutions, and standard antibiotics DMSO (as a negative control) and ampicillin (as a positive control) were placed and against the pathogenic bacterial strains on the inoculated agar.[19] Antibacterial activity was quantified by calculating the diameter of the clear zone of inhibition (ZOI) on the impervious contextual of microbial growth after cultivation at 37°C for 36 h in bacterial strains, and the average values of both assays were also calculated.

RESULTS AND DISCUSSION

XRD Analysis

The crystalline structure and phase purity of as-obtained pristine $CoWO_4$, CeO_2, and $CeO_2/CoWO_4$ NCs were determined by the XRD pattern. As displayed in Fig. 1, the pristine $CoWO_4$ sample displays the specific XRD diffraction peak of pure monoclinic system, space group P2/a and the emerge peak by 2θ values of 18.92°, 23.75°, 36.22°, 53.81° corresponding to the (010), (001), (111), (112) crystal plane of $CoWO_4$ (JCPDS file #15-0867).[20] Characteristic peaks at 2θ values of 28.55°, 32.97°, 47.54°, 56.26° could be indexed which correspond to (111), (200), (220), (311) crystallographic planes intense and well-suited diffraction peaks of cubic phase CeO_2 (JCPDS file #81-0792), respectively.[21] The diffraction peak is robust, which indicates that it has great crystallinity. While the $CeO_2/CoWO_4$

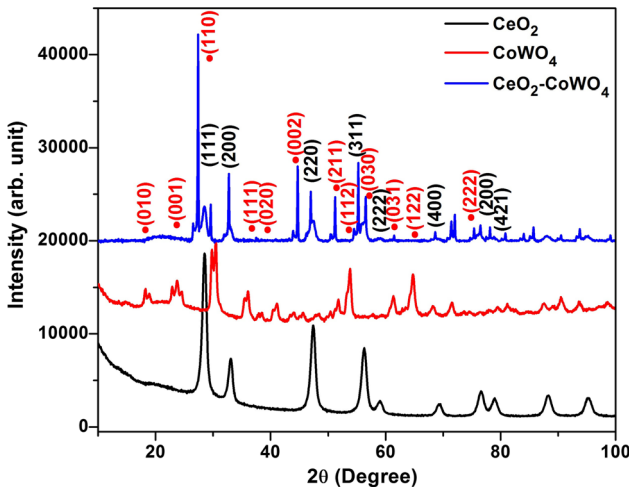

Fig. 1. XRD pattern of as-obtained CeO_2, $CoWO_4$ and $CeO_2/CoWO_4$ NCs.

NCs exposed the survival of diffraction peaks of together phases of $CoWO_4$ and CeO_2 and the diffraction peak lifted towards a minor angle, signifying that CeO_2 dropped/occurs in lattice oxygen space, indicating that CeO_2 has active packing on $CoWO_4$ lattice. Peaks interrelated to $CeO_2/CoWO_4$ heterojunction NCs are reliable with resultant separate, and no further any impurity specific peaks/phases could be observed, indicating the successful assembly of high-purity NCs/hybrid NMs. The average crystallite size of pristine $CoWO_4$, CeO_2, and $CeO_2/CoWO_4$ NCs was designed for the most intense peak since Debye–Scherrer's equation was established to be 23.5–28 nm, 27–30.4 nm and 25.2–19.05 nm, respectively. For now, the equation is $D = 0.9\lambda/\beta\cos\theta$, where D represents the crystallite size, λ stands for a wavelength of the used x-ray radiation (1.5418 Å), β is the full width at half maximum (FWHM) of the diffraction peak and θ is the scattering angle. Since the decline in crystallite size might be expressively repressed owing to the existence of $CoWO_4$ has abundant integration in the CeO_2 lattice.[22]

FTIR Spectral Analysis

FTIR analysis was conducted to gain a better understanding of the chemical structures, functional groups information of pristine CeO_2, $CoWO_4$ and $CeO_2/CoWO_4$ NCs over a frequency range of 4000–400 cm^{-1} as revealed in Fig. 2. The precise bands at 1045 and 1397 cm^{-1} were assigned to the individual peaks related to C=O and C–O stretching vibrations, respectively. The characteristic bands situated at 1544 cm^{-1} and 1625 cm^{-1} were consigned to different types of C–H vibration.[23] The notable bands at 574 cm^{-1} were usually recognized owing to the vibrational kind of Ce–O absorption bonding. Likewise, the bands observed at 748 cm^{-1}, 793 cm^{-1} and 892 cm^{-1} were attributed to deformation ways of Ce–O–Ce, Co–O and W–O bonds by chain stretching vibrations, respectively. The extreme bands perceived at about 3367 cm^{-1} and 1548 cm^{-1} were owing to O–H stretching vibrations kind (H-bonded) of inside bonded or surface adsorbed hints of residual water (H_2O), and the oxygen (O–) functionalities individually.[24]

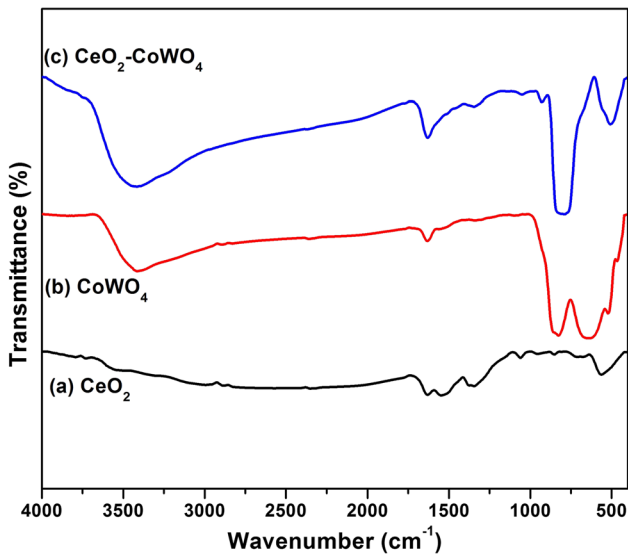

Fig. 2. FTIR spectra of (a) CeO_2 (b) $CoWO_4$ and (c) $CeO_2/CoWO_4$ NCs.

Surface Morphology and Elemental Mapping

The surface morphology of the as-ascribed pristine CeO_2, $CoWO_4$, and $CeO_2/CoWO_4$ NMs samples was determined by HR-SEM images as shown in Fig. 3a, b, and c. All the as-obtained sample display highly agglomerated sphere-like NSs which indicate the satisfactory foundation of NPs.[12,25] The elemental purity of the $CeO_2/CoWO_4$ NCs was established via the EDX system. As demonstrated in the EDX peaks shown in Fig. 3d, the $CeO_2/CoWO_4$ NCs are composed of Ce, W, O, and Co elements. Besides, no further impurity peaks were observed, which indicates positive configuration[26] with a high purity level of as-obtained $CeO_2/CoWO_4$ NCs, and the relative element/content weight ratios are indicated in the table (inset Fig. 3d). Further details of the $CeO_2/CoWO_4$ heterojunction NCs are recognized via EDX mapping, as depicted in Fig. 4. Figure 4a–e reveals the sample expanse for EDX mapping, illuminating the dispersal of Ce, W, O, and Co elements in Fig. 4b, c, d, and e relatively. Besides, the Ce, W, O, and Co elements have an identical circulation of the Ce and O reactive species on the surface/boundary of $CoWO_4$ NPs.[27]

HRTEM was used to further characterize the features of deepness morphology, crystalline nature and particle size of as-obtained NCs. Figure 5a shows the high-magnification image of $CeO_2/CoWO_4$ NCs, and it is observed that quasi-spherical NPs are well dispersed and adhere to one another.[3,9] The as-organized $CeO_2/CoWO_4$ NCs by average sizes in the range of nearly ~ 25–29 nm in attendance of an effective hydrothermal heating way. Likewise, the selected area electron diffraction (SAED) outlines (inset of Fig. 5b) show that the vibrant lattice fringes stable mutually, which confirms the good construction of interfacial assembly among the $CoWO_4$ and CeO_2 NPs in the composite also specifying random directions, which is highly consistent with the XRD outcome, indicating that the photo-excited charge carrier (e^-–h^+) effort between the $CeO_2/CoWO_4$ NCs.[28]

UV–Vis DRS Absorption Spectra

As is well recognized, the photocatalytic activity of a photocatalyst is determined via the light absorption capability. The optical absorption properties of pristine CeO_2, $CoWO_4$ NPs, and $CeO_2/CoWO_4$ NMs were clarified by UV-DRS spectra as shown in Fig. 6a. The strong absorption region observed at 290–400 nm was characteristic of CeO_2

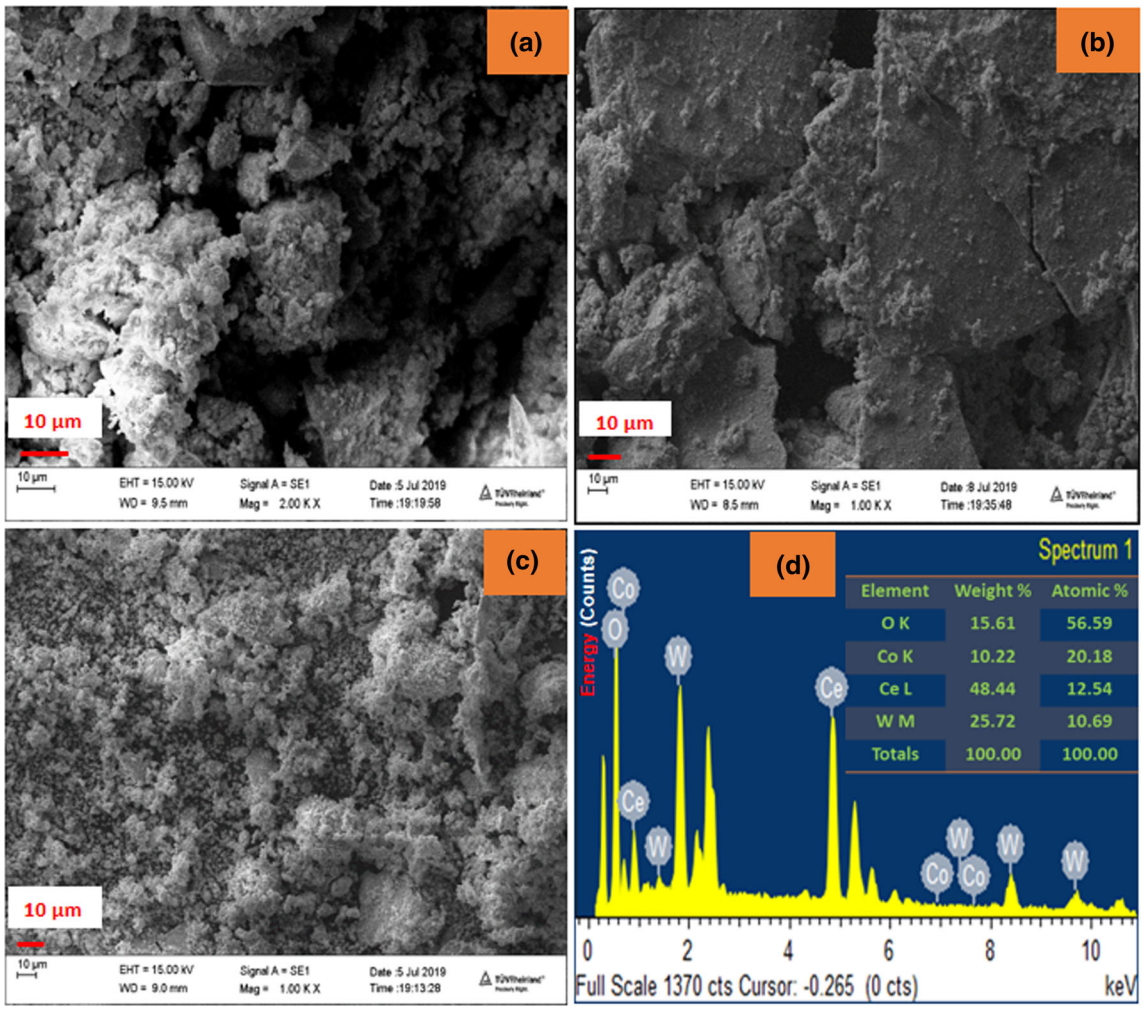

Fig. 3. HR-SEM images of (a) CeO_2 (b) $CoWO_4$ (c) $CeO_2/CoWO_4$ and (d) EDAX spectra of $CeO_2/CoWO_4$ NCs.

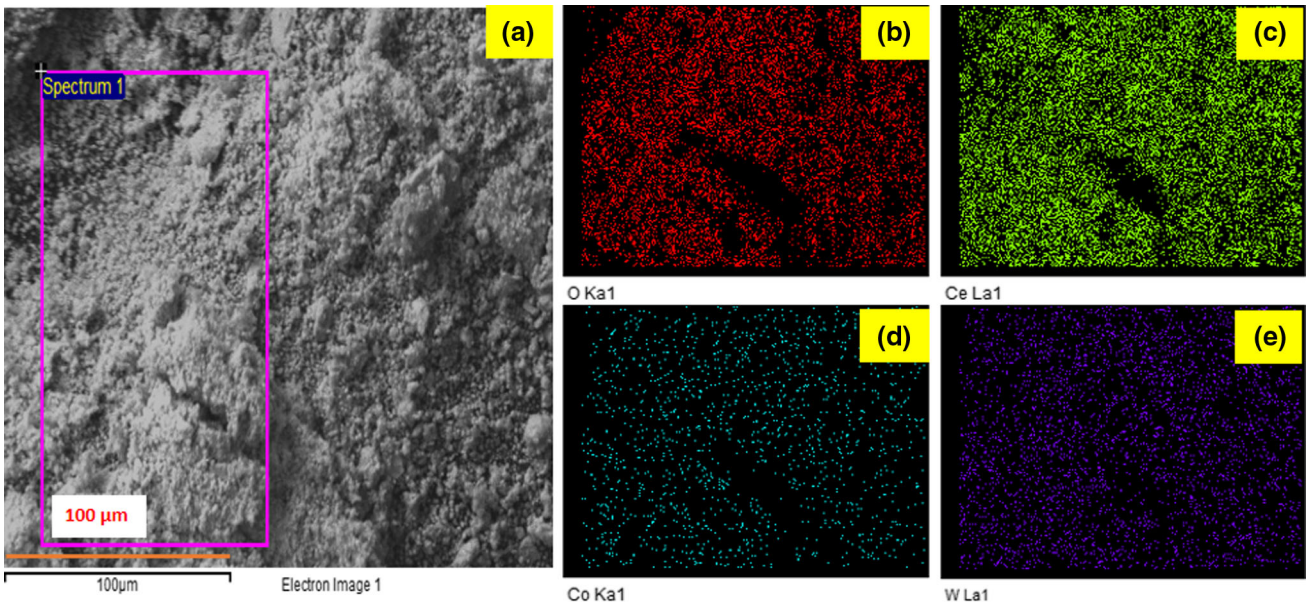

Fig. 4. Elemental mapping for (a) specified HR-SEM image of $CeO_2/CoWO_4$ NCs and relative, (b) Ce, (c) W, (d) O, and (e) Co elements respectively.

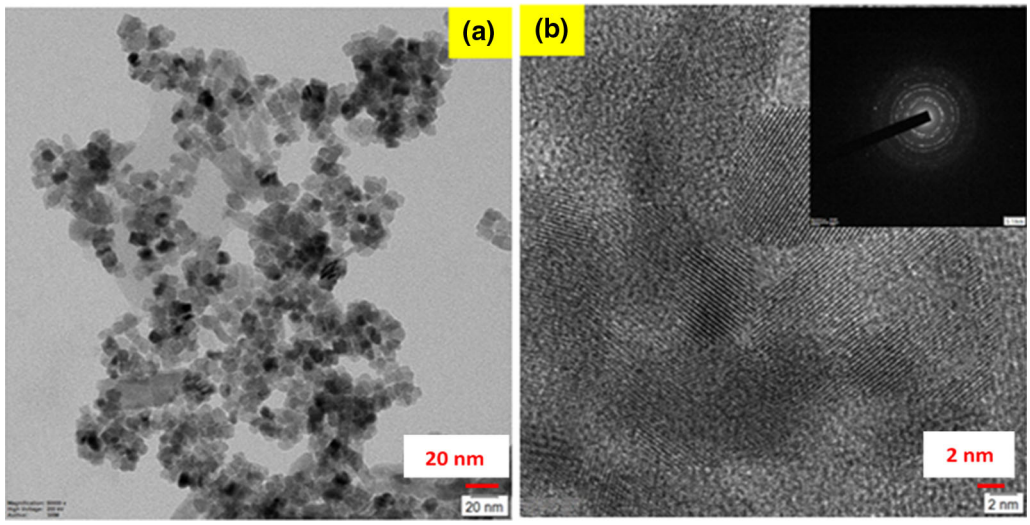

Fig. 5. (a) 20 nm and (b) 2 nm magnification HR-TEM images of as-obtained $CeO_2/CoWO_4$ NCs.

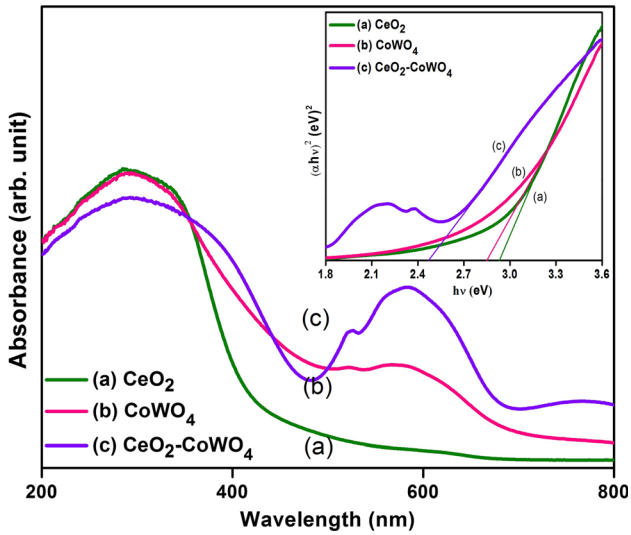

Fig. 6. UV–Vis DRS spectra and (inset) Band gap energy of as-obtained nanomaterials.

and $CoWO_4$ NMs. The absorbance edges of pristine CeO_2 and $CoWO_4$ NMs are situated at about 292 nm and 295 nm, respectively. By adapting to mixing with the $CeO_2/CoWO_4$ NCs at the absorbance edges ($\sim$ 296 nm, 465 nm) consume strong visible-light absorption further effectively than further as-obtained NMs, though auxiliary red-shifted light absorption capability with great mediate between $CoWO_4$ and CeO_2. These results suggest that the as-obtained PCs would retain visible-light photocatalytic activity.[29] The bandgap energy of the PCs can be calculated via the Tauc equation by the following formula:[30] $\alpha h\nu = A(h\nu - E_g)^{n/2}$, where α stands for the absorption coefficient, $h\nu$ stands for photon energy, E_g represents the bandgap, and A is a proportionality constant, respectively. The value of n is determined by the type of optical transition of the semiconductor (i.e., n = 1 for directly allowable transition and n = 4 for indirectly allowable transition). Using the optical absorption data and the Tauc equation, the energy gap values of pristine CeO_2, $CoWO_4$, and $CeO_2/CoWO_4$ NCs are 2.92 eV, 2.83 eV and 2.46 eV, respectively (Fig. 6b). The bandgap energies decreased in the composite on mixing of $CeO_2/CoWO_4$, which may reflect the synergistic influence of the interaction between CeO_2 and $CoWO_4$ NPs leading to the smaller bandgap energy similarly increasing the visible-light absorption aptitude.[31] It was itemized that the well-suited overlying band-structure in the composite could facilitate the separation/charge-transfer of electron–hole (e^-–h^+) pairs, thus suggesting that $CeO_2/CoWO_4$ NCs improve the photocatalytic activity for the removal of organic impurities under visible-light exposure.[32]

Photoluminescence (PL) Properties

To characterize the trapping, charge migration, excitation properties, and separation efficiency of photo-excited charge carriers of the as-attained samples, they were further investigated by via PL emission spectra inquiry.[33] The room-temperature PL spectra of the $CeO_2/CoWO_4$ heterojunction NCs, pristine CeO_2, and $CoWO_4$ NPs are shown in Fig. 7. In Fig. 7, it can be seen that the PL emission intensity of $CeO_2/CoWO_4$ is lower than that of pristine CeO_2 and $CoWO_4$ NPs. Speciously the outline of $CoWO_4$ NPs indicated a strong emission peak at $\sim$ 428 nm, 446 nm and 478 nm, the $CeO_2/CoWO_4$ sample exposed clearly decreased PL intensity, which indicates that the heterojunction reserved via blending with CeO_2 and $CoWO_4$ NPs results in a strangely hindered recombination rate of photoexcited (e^-–h^+) pairs, thus enhancing the photocatalytic performance.[34] The effects also signify the improved charge separation ability owing to

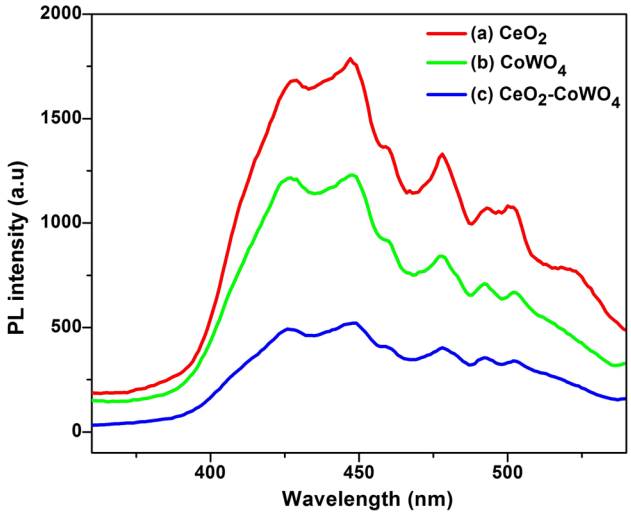

Fig. 7. Room-temperature PL spectra of as-obtained nanomaterials.

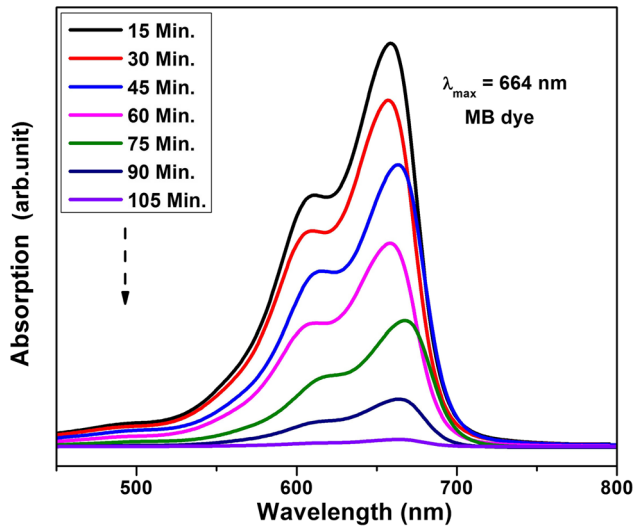

Fig. 8. UV-Vis absorption spectra of MB dye degradation of CeO_2/$CoWO_4$ NCs.

the transfer of photoelectrons (e^-) across the boundary of CeO_2 and $CoWO_4$ pairing materials.

Photocatalytic Performance Under Visible-Light Treatment

The photocatalytic activity of the as-obtained samples was estimated via the aqueous MB dye photodegradation by visible-light exposure. Figure 8 shows that the consistent UV–Vis absorption spectrum of MB dye photodegradation with CeO_2/$CoWO_4$ PCs was rationally executed. In addition, on the CeO_2/$CoWO_4$ PCs, it virtually entirely disappeared after light exposure for 105 min. The pristine CeO_2 exhibited the lowest photocatalytic activity (41%), and $CoWO_4$ also showed a low degradation ratio of around 52.5%. Conversely, the CeO_2/$CoWO_4$ coupled NCs showed outstanding photocatalytic performance for MB dye photodegradation, which was superior to the other as-obtained samples. After 105 min exposure to visible light, the CeO_2/$CoWO_4$ sample demonstrated the highest photocatalytic activity, with 92.5% of dye degraded under similar settings.[35] The self-degradation/straight photolysis of the dye have less than 2% after 105 min of light exposure, later agreeing it to be ignored. The decomposition efficacy of MB dye is projected by the following expression: Decomposition% = $C_0 - C/C_0 \times 100$, where C_0 and C_t are the primary concentration of MB dye and the equilibrium concentration through the reaction, respectively.[36] The relationship between concentration ratios (C_t/C_0) on light exposure time is displayed in Fig. 9a. The photodegradation efficiency (Fig. 9b) of these catalysts was found to be in the following order: CeO_2/$CoWO_4$ > $CoWO_4$ > CeO_2. This greater photocatalytic performance is attributed to the significantly improved photoactivity, fortunate photoexcited charge transfer, and visible-light absorption facility for CeO_2/$CoWO_4$ PCs initiated via the sensitive influence of environmental remediation. The heterojunction NCs similarly inhibit the photo-excited (e^-–h^+) recombination, which may be ascribed to the developed charge separation efficiency between the coupled $CoWO_4$ and CeO_2 catalyst surface, enabling better visible-light absorption, which hence enhances the visible-light photocatalytic performance.[37]

Additionally, by the resolution of better compare/defend the photocatalytic activity and photodegradation rate kinetics of MB dye considered over the as-invented samples surveyed the pseudo-first-order kinetic model (Fig. 10). Also, ln $C_0/C_t = kt$, where k represents the first-order rate constant plotted from a graph, C_0 symbolizes the initial concentration and C_t represents the concentration of MB dye with exposure time t of visible light.[38] It was observed that CeO_2/$CoWO_4$ PCs have a maximum rate constant of 0.04212 min^{-1}, nearly 3.1-fold and 1.23-fold greater than pristine CeO_2 (0.0134 min^{-1}) and $CoWO_4$ (0.0343 min^{-1}), respectively. According to the outcomes, the photodegradation rate of MB aqueous dye was significantly increased owing to the momentous manipulating statistic that the synergistic upshot of effects of the combination of $CoWO_4$ and CeO_2 NMs present in the NCs. Upon exposure of CeO_2 NPs to visible light, the separation of photoelectrons (e^-) from the conduction band (CB) facilitated the rapid transport to the $CoWO_4$, which helped to prevent/hinder the foundation of photo-generated (e^-–h^+) pair recombination and causing holes (h^+) in the valence band (VB) of CeO_2 NPs, leading to the improved photocatalytic performance.[22,39] Lastly, the photo-excited e^- and h^+ could react with H_2O to generate OH^- radicals and oxygen species rather than to degrade the dye molecules.

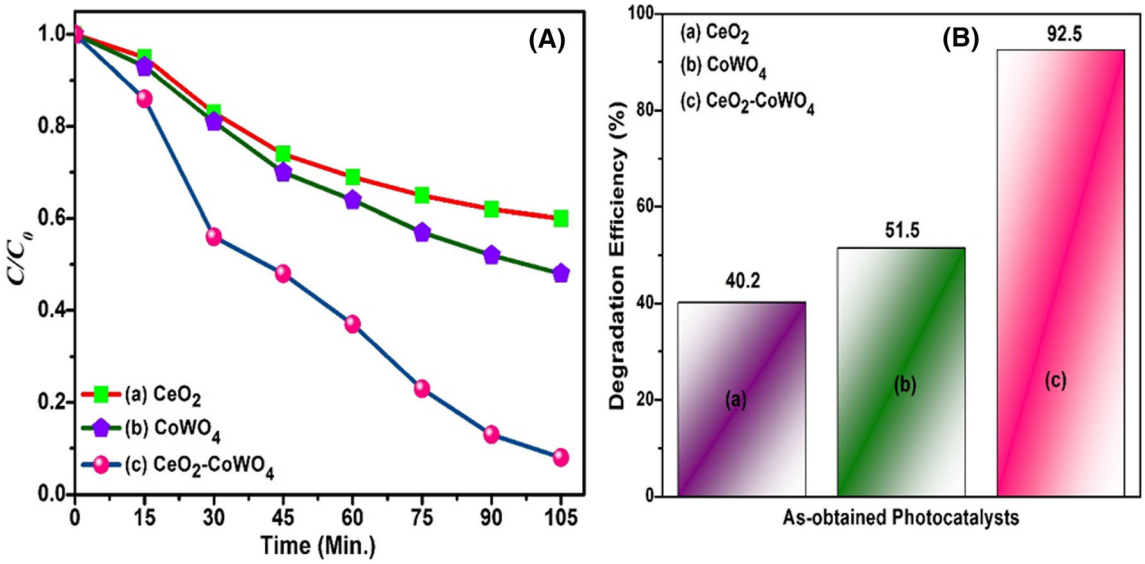

Fig. 9. (A) Photodegradation of MB dye over the (a) CeO_2 (b) $CoWO_4$ (c) $CeO_2/CoWO_4$ PCs. (B) Degradation efficiency of MB dye by (a) CeO_2 (b) $CoWO_4$ (c) $CeO_2/CoWO_4$ PCs.

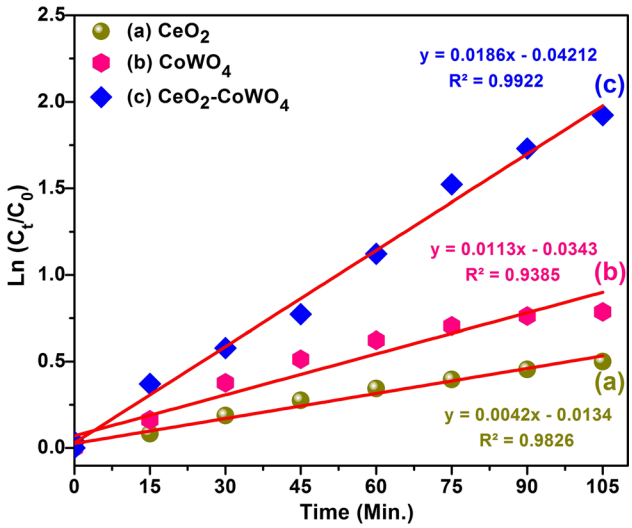

Fig. 10. First-order kinetic plot for the degradation of MB over the as-obtained PCs.

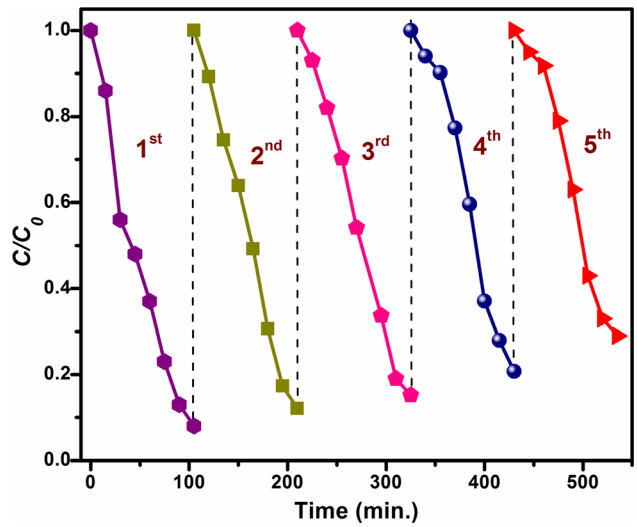

Fig. 11. Five repetitive recycling processes of $CeO_2/CoWO_4$ PCs for photodegradation of MB dye under visible-light exposure.

Reusability Test

The reusability and stability of the photocatalyst NMs are further essential qualities in real-time applications. Successive runs of aqueous MB dye over the $CeO_2/CoWO_4$ active PCs under visible light were carried out to evaluate its stability (Fig. 10b). Respectively cyclic runs recuperate well again the photocatalyst via centrifugation with further washed numerous times with DI water and dried, and the recovered PCs were then used for the successive catalytic runs.[40] As shown in Fig. 11, there is no deceptive reduction of photodegradation effectiveness during five reusability cycles, with a slight decrease in efficiency from 92.5% in the first run to 81% in the fifth run. This decreased photodegradation efficiency is ascribed to the photo-dissolution and photo-corrosion of the as-obtained catalyst. In addition, the XRD patterns and FTIR spectra of the $CeO_2/CoWO_4$ NC before and after five repeated runs are displayed in Fig. 12a and b. Hence, there was no evident variance among the intact PCs, establishing that the coupling of $CoWO_4$ and CeO_2 NMs can effectively inhibit the recombination of photoexcited (e^-–h^+) charges to a large degree, and confirming the good stability and robustness of $CeO_2/CoWO_4$ PCs. Thus, the results verify that the $CeO_2/CoWO_4$ photocatalyst possesses excellent stability and recyclability, and is a good candidate for practical photocatalytic applications.[41–43] The photodegradation and photoactivity of the $CeO_2/CoWO_4$ catalyst were also compared with several nanocomposite materials,[44–48] and the results are given in Table I.

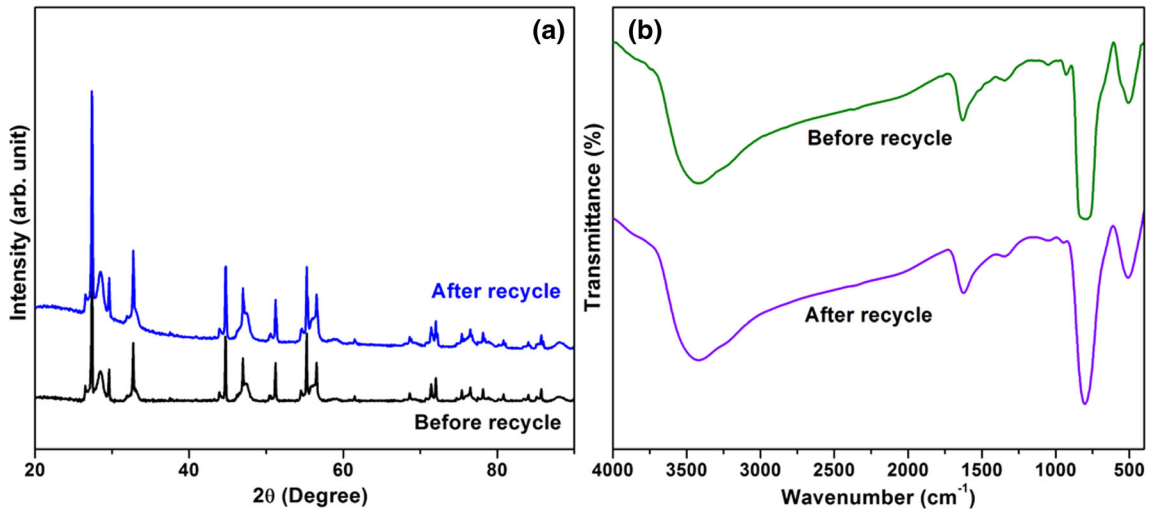

Fig. 12. (a) XRD pattern and (b) FTIR spectra for $CeO_2/CoWO_4$ PCs before and after a photocatalytic reaction.

Table I. Comparison of visible-light-assisted MB photodegradation rate (%) with that of previously reported nanomaterials

S. no.	Catalyst	Irradiation time (min)	Degradation efficiency (%)	References
1.	CdS/TiO_2	310	62	[44]
2.	CeO/ZnO	150	97	[45]
3.	ZnO/SnO_2	240	100	[46]
4.	rGO/ZnO	90	99	[47]
5.	$SnO_2/ZnO/TiO_2$	300	27	[48]
6.	CeO_2-$CoWO_4$	105	92.5%	This work

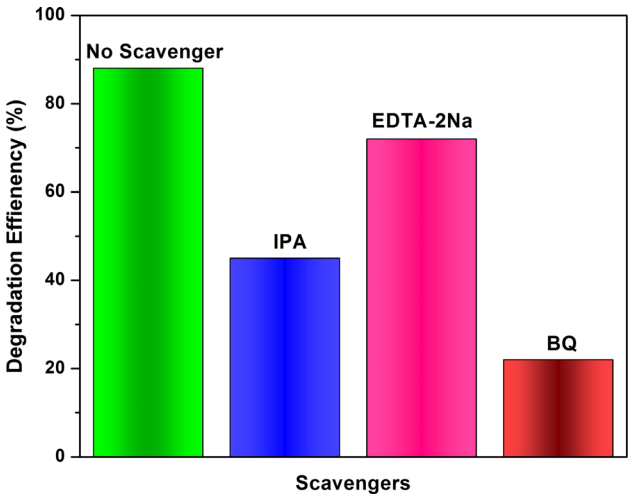

Fig. 13. Effects of different scavengers on the degradation of MB dye in the presence of $CeO_2/CoWO_4$ PCs.

Detection of Reactive Species and the Photocatalytic Mechanism

To examine the photocatalytic mechanisms of the $CeO_2/CoWO_4$ heterojunction photocatalyst, different scavengers were presented to recognize the influences of one or further intermediary reactive/oxidative species ($^{\cdot}OH^-$, $O_2^{\cdot-}$ and h^+) in a photocatalytic manner. As illustrated in Fig. 13, once BQ was added, the degradation performance of MB aqueous dye decreased from 88.5% to 23%, signifying that the $\cdot O_2^-$ played a dynamic role in photodegradation.[49] Equally, a momentous loss of photo-decomposition (45%), whereas the addition of IPA, proving that the $\cdot OH^-$ pathway played a decisive role in the degradation process. Moreover, when EDTA-2Na was added in a photocatalytic mode, the degradation efficacy of dye was slightly depressed, specifying that little holes (h^+) were only involved also it has not a crucial provider in the photodegradation progression of MB dye subtraction. As an effect, it might be resolved that $^{\cdot}O_2^-$ and $^{\cdot}OH^-$ were central donated roles of reactive species in the photocatalytic route in visible-light exposure.[50,51]

Based on the above experimental and the theoretical analysis, a projected energy band structure of the $CeO_2/CoWO_4$ PCs is illustrated schematically in Fig. 14. The CB and VB edge potential (versus NHE)[52] of $CeO_2/CoWO_4$ PCs at the point of zero charge was determined using Mulliken electronegativity Eqs. 1 and 2:

$$E_{VB} = X - E_e + 0.5E_g \quad (1)$$

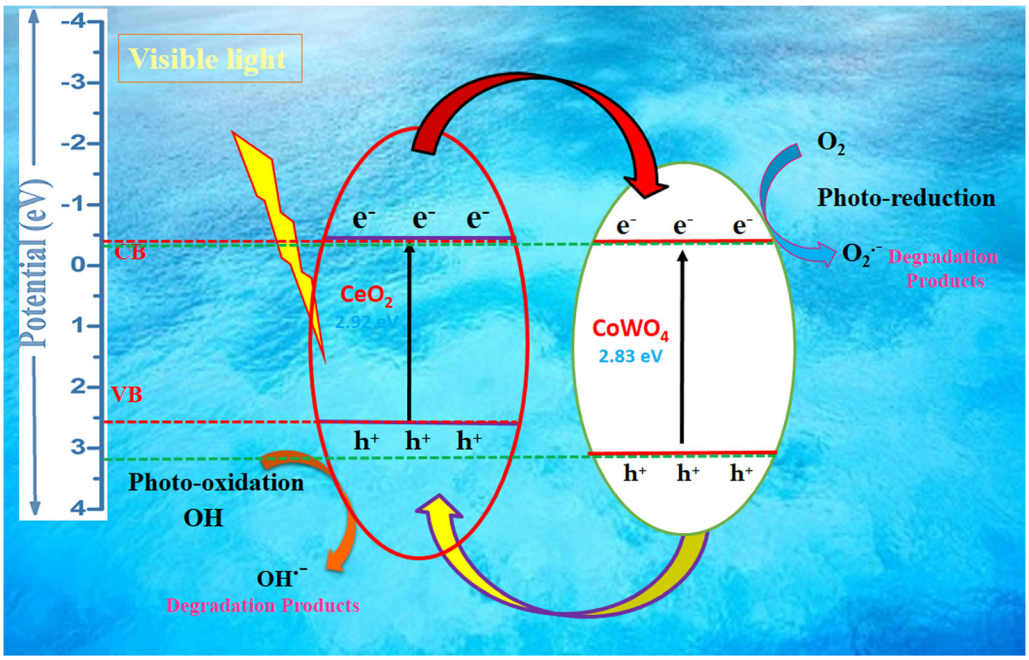

Fig. 14. The plausible mechanism of the MB dye degradation for CeO2/CoWO4 PCs.

$$E_{CB} = E_{VB} - E_g \quad (2)$$

wherever χ is the absolute electronegativity of the semiconductor (χ is 5.56 eV, 6.32 eV for CeO_2 and $CoWO_4$, respectively). E_e stands the free electron energy of the hydrogen scale (4.5 eV) values and E_g is the bandgap of the obtained semiconductor.[53] The intended E_{CB} and E_{VB} of CeO_2 were − 0.40 eV and 2.52 eV, and of $CoWO_4$ were − 0.405 eV and 3.23 eV, respectively. According to the UV-DRS results, when the $CeO_2/CoWO_4$ PCs system was exposed under visible light (> 400 nm), together CeO_2 and $CoWO_4$ could be stimulated since the energy gap of CeO_2 and $CoWO_4$ observed in this analysis were 2.92 eV and 2.83 eV.

To understand the reason for this enhanced performance, a plausible photocatalytic mechanism for the photodegradation of MB dye over the $CeO_2/CoWO_4$ PCs is depicted in Fig. 13. From this analysis, one can easily see that the CeO_2 not only plays sustenance but similar activity as the ligands, which helps to increase the separation efficacy of the photoexcited (e^-–h^+) pairs.[54] Linking $CoWO_4$ and CeO_2 with different bandgap to form composite NMs are further flexible than fixing for extending the light absorption and fewer thoughtful to the constituent homogeneity.[55,56] As visible light provided the surface of $CeO_2/CoWO_4$ PCs with adequate energy, h^+ and e^- were photoexcited in the VB and CB hereafter be the boundary part series of reactions generating reactive radical species. However, photoexcited h^+ gathered at the VB, edge potential of $CoWO_4$ (3.23 eV versus NHE) reacted by H_2O to give rise to $^{\cdot}OH^-$ radicals, which was the photo-oxidation progression leading to increased charge separation. The photo-excited (e^-) at the CB edge potential of CeO_2 (− 0.40 eV versus NHE) crystallites are transported to the CB of $CoWO_4$ (− 0.405 eV versus NHE) has less negative than the typical redox potential of crystallites. Conversely, the photoexcited (e^-) on illumination to the CB of $CeO_2/CoWO_4$ PCs with the adsorbed oxygen softened in aqueous medium might ease O_2 to yield $^{\cdot}O_2^-$ species.[57,58] could respond through MB dye and despoiled it into CO_2 and H_2O. Moreover, these $^{\cdot}O_2^-$ radicals respond with H_2O were contributed in the redox response fashioned which eventually caused $^{\cdot}OH^-$ radicals and the VB of h^+ is apprehended by H_2O or respond with a generation of OH groups to form the surface $^{\cdot}OH^-$ radicals which oxidized the dye impurities in visible-light. Thus, the photocatalytic reactivity, the $CeO_2/CoWO_4$ composite indicates effective segregation of photoexcited (e^-–h^+) charge-carrier, thus developed photosensitization and photocatalytic reactivity could be successfully realized.[59] The plausible solutions concerning the above-reference substance are expressed below (Eqs. 3, 4, 5, 6, and 7).

$$CeO_2/CoWO_4 + Dye + Light \rightarrow CeO_2/CoWO_4 + Dye + (e^-(CB) + h^+(VB)) \quad (3)$$

$$Dye + OH \rightarrow OH^{\cdot -} + DegradationProducts \quad (4)$$

$$Dye + O_2 \rightarrow O_2^{\cdot -} + DegradationProducts \quad (5)$$

$$Dye + e^-(CB) \rightarrow ReductionProducts \quad (6)$$

$$Dye + h^{+}(VB) \rightarrow OxidativeProducts \qquad (7)$$

Antibacterial Experiments

Essential oils are capable of use as regular antimicrobial agents; however, the modest solubility and infrequent biological situations confine their use against bacteria in biofilm and dispersed sites together,[60] since here as-organized NCs have been used for antibacterial agents. Antibacterial activity of $CeO_2/CoWO_4$ NCs was measured against gram-negative *E. coli* and gram-positive *S. aureus* pathogenic bacterial strains by the agar well diffusion method. Figure 15 clearly shows the zone of inhibition (ZOI) at different concentrations (25 μg/mL, 50 μg/mL and 75 μg/mL) of $CeO_2/CoWO_4$, $CoWO_4$, and CeO_2 for the typical control which directed the antibacterial outcome.[61] The antibacterial activity of as-obtained catalysts against the pathogenic bacterial strains by different concentrations is shown in Table II. The superior antibacterial activity of the as-attained $CeO_2/CoWO_4$ NCs at a concentration of 75 μg/mL consumed a capable antibacterial influence beside gram-positive of *S. aureus* bacteria through a ZOI value of ~6.5–9 mm on equating by the typical drug of DMSO. Moreover, the combined $CoWO_4/CeO_2$ indicated that the NCs collected round the surface membranes, which might respond with the microbial membranes and produced internalization of the NCs in the microbe's cells.[62] The use of efficient gold (Au) NPs has to contest multi-drug-resisted pathogenic bacteria. For regulation of the functional pairs on the as-obtained NPs surface has if gold NPs that were active besides both gram-positive and gram-negative bacterial strain, comprising that multi-drug-resistant pathogen similarly.[63] Antibacterial effectiveness of the fascinatingly triggered LM NPs was measured besides both the Gram-negative and Gram-positive microbial biofilms moderately. After 90 min, over 99% of both microbial species suited nonviable, and the degradation of the attained active biofilms was perceived.[64] The mechanism for the bactericidal motion of NPs appearances substantial efficacy for the responsive/reactive oxygen species (ROS) and its bactericidal strains actual part in its metallic NPs and their complexes in the existence of oxygen species and accordingly[65] donate to the superior mechanical damage for the utilities of microbes, and enhanced bactericidal effects of hybrid $CoWO_4/CeO_2$ nanostructured materials. Moreover, the greater

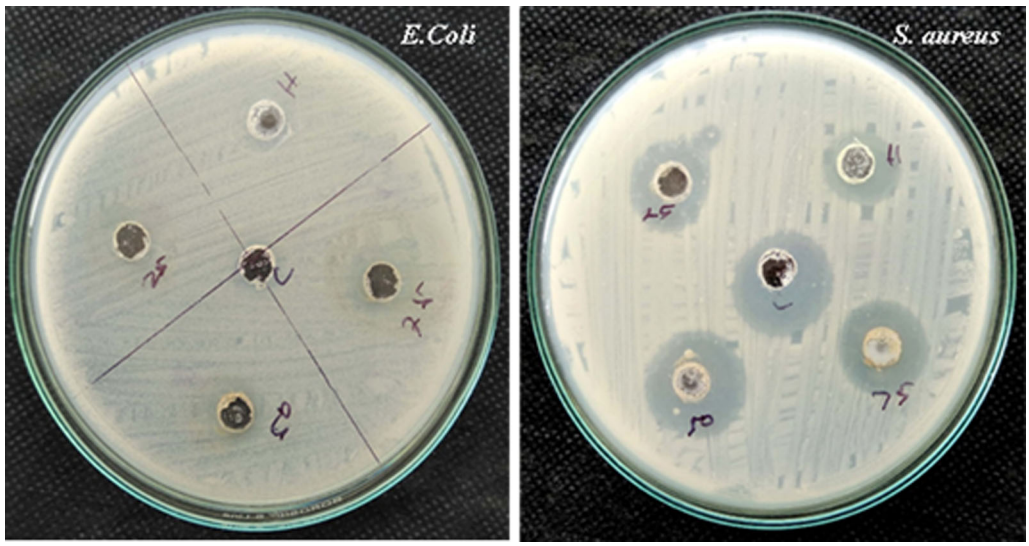

Fig. 15. Antibacterial ZOI value by *E. coli* and *S. aureus* bacteria of as-prepared $CeO_2/CoWO_4$ nanomaterials.

Table II. Assessment on the zone of inhibition of antibacterial activity for as-prepared nanoparticles

		Zone of inhibition range (mm)					
		E. Coli			*S. aureus*		
S. no.	**Microorganisms**	**25 μg**	**50 μg**	**75 μg**	**25 μg**	**50 μg**	**75 μg**
1.	CeO_2	2 ± 0.5	2.5 ± 1	3.5 ± 0.5	3 ± 1	6 ± 1	7 ± 1
2.	$CoWO_4$	2 ± 1	2 ± 0.5	3 ± 0.3	3.5 ± 1	6.5 ± 0.5	8.5 ± 0.5
3.	CeO_2-$CoWO_4$	3.5 ± 0.5	3.5 ± 0.5	4 ± 1.5	6.5 ± 0.5	8 ± 0.5	11 ± 0.5

concentration of all these managed NCs materials are destructive to both the consumers and microorganisms; however, nano-level concentrations of these NMs are further applications for the destruction of microbes.[66,67]

SUMMARY AND CONCLUSION

In summary, a novel $CeO_2/CoWO_4$ heterostructured NCs photocatalyst was successfully prepared via a facile hydrothermal-based process. The assembly of effective NCs was characterized via XRD, HRTEM, UV-DRS, PL spectra, and photocatalytic analysis. The $CeO_2/CoWO_4$ NCs by agglomeration virtually spherical fashioned morphology with an average size of approximately 25–29 nm, likewise revealed admirable optical properties and energy bandgap value of 2.46 eV. The photocatalytic assessment of $CeO_2/CoWO_4$ PCs indicated clearly superior photodegradation efficiency against an aqueous MB dye solution, i.e. 92.5% within 105 min of visible-light treatment, in comparison with the $CoWO_4$ and CeO_2 NPs. Additionally, the $CeO_2/CoWO_4$ PCs confirmed good recyclability and high stability during five cycles, and thus can be reused. The improved photoactivity of $CeO_2/CoWO_4$ PCs was attributed to the improved light-harvesting efficiency, actual transfer, and separation of photo-excited (e^-–h^+) pairs owing to proper energy band potentials amid the synergistic effects of the interaction of $CoWO_4$ and CeO_2 NPs. The $^{\cdot}O_2^-$ and $^{\cdot}OH^-$ were responsible for the effectual reactive species to removal and mineralization through the degradation manner. The feasible mechanism behind in the photodegradation of MB dye in the presence of $CeO_2/CoWO_4$ PCs was then defined. Likewise, the synthesized $CeO_2/CoWO_4$ NCs expression the momentous influence on the antibacterial activity against pathogenic bacterial strains. This work may offer an efficient new platform for the well-ordered stable $CeO_2/CoWO_4$ heterostructured PCs, which facilitates great efficient solar energy conversion to resolve key environmental issues with regard to wastewater effluence remediation.

CONFLICT OF INTEREST

The authors declare that they have no conflict of interest.

ACKNOWLEDGMENTS

The authors thank the Department of Physics & Nanotechnology, SRM Institute of Science and Technology, Kanchipuram, Tamil Nadu, India for TEM measurement.

REFERENCES

1. A. Paul Chowdhury, and B.H. Shambharkar, *Int. J. Appl. Ceram. Technol.*, 2020, 17, p 1467.
2. Z. Shu, Y. Zhang, J. Ouyang, and H. Yang, *Appl. Surf. Sci.*, 2017, 420, p 833.
3. S.M. AlShehri, J. Ahmed, A.M. Alzahrani, and T. Ahamad, *New J. Chem.*, 2017, 41, p 8178.
4. J. Ke, M. Adnan Younis, Y. Kong, H. Zhou, J. Liu, L. Lei, and Y. Hou, *Nano Micro Lett.*, 2018, 10, p 69.
5. M.A. Subhan, T. Ahmed, N. Uddin, A.K. Azad, and K. Begum, *Spectrochim. Acta Part A Mol. Biomol. Spectrosc.*, 2015, 136, p 824.
6. M.M. Rashad, A.A. Ismail, I. Osama, I.A. Ibrahim, and A.-H.T. Kandil, *Arab. J. Chem.*, 2014, 7, p 71.
7. K. Sujatha, T. Seethalakshmi, A.P. Sudha, and O.L. Shanmugasundaram, *Nano Struct. Nano Objects*, 2019, 18, p 100305.
8. M. Nadeem, R. Khan, K. Afridi, A. Nadhman, S. Ullah, S. Faisal, Z.U. Mabood, C. Hano, and B.H. Abbasi, *Int. J. Nanomed.*, 2020, 15, p 5951.
9. Z. Cui, H. Zhou, G. Wang, Y. Zhang, H. Zhang, and H. Zhao, *New J. Chem.*, 2019, 43, p 7355.
10. N. Wetchakun, S. Chaiwichain, B. Inceesungvorn, K. Pingmuang, S. Phanichphant, A.I. Minett, and J. Chen, *ACS Appl. Mater. Interfaces*, 2012, 4, p 3718.
11. K. Jothivenkatachalam, S. Prabhu, A. Nithya, S. Chandra Mohan, and K. Jeganathan, *Desalin. Water Treat.*, 2015, 54, p 3134.
12. F. Ahmadi, M. Rahimi-Nasrabadi, A. Fosooni, and M. Daneshmand, *J. Mater. Sci. Mater. Electron.*, 2016, 27, p 9514.
13. V. Shanmugam, K.S. Jeyaperumal, P. Mariappan, and A.L. Muppudathi, *New J. Chem.*, 2020, 44, p 13182.
14. Z. Li, D. Liu, W. Huang, Y. Sun, S. Li, and X. Wei, *Surf. Interface Anal.*, 2019, 51, p 336.
15. X. Yan, Z. Wu, C. Huang, K. Liu, and W. Shi, *Ceram. Int.*, 2017, 43, p 5388.
16. D. Madhan, P. Rajkumar, P. Rajeshwaran, A. Sivarajan, and M. Sangeetha, *Appl. Phys. A*, 2015, 120, p 463.
17. A.B. Ali Baig, V. Rathinam, and J. Palaninathan, *Appl. Water Sci.*, 2020, 10, p 76.
18. A. Akbari-Fakhrabadi, R. Saravanan, M. Jamshidijam, R.V. Mangalaraja, and M.A. Gracia, *J. Saudi Chem. Soc.*, 2015, 19, p 505.
19. Z. Nasir, M. Shakir, R. Wahab, M. Shoeb, P. Alam, R.H. Khan, and M. Mobin, *Int. J. Biol. Macromol.*, 2017, 94, p 554.
20. Z. Liu, J. Xu, Y. Li, and H. Yu, *Catal. Lett.*, 2018, 148, p 3205.
21. L.S. Reddy Yadav, K. Lingaraju, B. Daruka Prasad, C. Kavitha, G. Banuprakash, and G. Nagaraju, *Eur. Phys. J. Plus*, 2017, 132, p 239.
22. S. Li, S. Hu, W. Jiang, Y. Liu, Y. Zhou, J. Liu, and Z. Wang, *J. Colloid Interface Sci.*, 2018, 530, p 171.
23. M. Jayanthi, T. Lavanya, N.A. Saradha, K. Satheesh, S. Chenthamarai, and R. Jayavel, *J. Nanosci. Nanotechnol.*, 2018, 18, p 3257.
24. P. Taneja, S. Sharma, A. Umar, S.K. Mehta, A.O. Ibhadon, and S.K. Kansal, *Mater. Chem. Phys.*, 2018, 211, p 335.
25. H. Cui, B. Li, Y. Zhang, X. Zheng, X. Li, Z. Li, and S. Xu, *Int. J. Hydrog. Energy*, 2018, 43, p 18242.
26. B. Maddah, F. Jookar-Kashi, and M. Akbari, *J. Mater. Sci. Mater. Electron.*, 2018, 29, p 13723.
27. R. Pandiyan, S. Mahalingam, and Y.-H. Ahn, *J. Photochem. Photobiol. B*, 2019, 191, p 18.
28. H. Balavi, S. Samadanian-Isfahani, M. Mehrabani-Zeinabad, and M. Edrissi, *Powder Technol.*, 2013, 249, p 549.
29. Y. Zhao, T. Chen, R. Ma, J. Du, and C. Xie, *Micro Nano Lett.*, 2018, 13, p 1394.
30. S.L. Prabavathi, K. Govindan, K. Saravanakumar, A. Jang, and V. Muthuraj, *J. Ind. Eng. Chem.*, 2019, 80, p 558.
31. X. Wang, W. Su, X. Hu, H. Liu, M. Sheng, and Q. Zhou, *Mater. Res. Express*, 2018, 6, p 35507.
32. S. Pourmasoud, M. Eghbali-Arani, F. Ahmadi, and M. Rahimi-Nasrabadi, *J. Mater. Sci. Mater. Electron.*, 2017, 28, p 17089.
33. H. Yang, B. Xu, S. Yuan, Q. Zhang, M. Zhang, and T. Ohno, *Appl. Catal. B*, 2019, 243, p 513.
34. B. Singaram, K. Varadharajan, J. Jeyaram, R. Rajendran, and V. Jayavel, *J. Photochem. Photobiol. A*, 2017, 349, p 91.

35. S. Feizpoor, and A. Habibi-Yangjeh, *J. Colloid Interface Sci.*, 2018, 524, p 325.
36. L. Wang, J. Ding, Y. Chai, Q. Liu, J. Ren, X. Liu, and W.-L. Dai, *Dalton Trans.*, 2015, 44, p 11223.
37. A. Priyadharsan, V. Vasanthakumar, S. Karthikeyan, V. Raj, S. Shanavas, and P.M. Anbarasan, *J. Photochem. Photobiol. A*, 2017, 346, p 32.
38. S. Kumar, and A.K. Ojha, *RSC Adv.*, 2016, 6, p 8651.
39. Q. Qiao, K. Yang, L.-L. Ma, W.-Q. Huang, B.-X. Zhou, A. Pan, W. Hu, X. Fan, and G.-F. Huang, *J. Phys. D Appl. Phys.*, 2018, 51, p 275302.
40. J. Zhang, L.-L. Peng, Y. Tang, and H. Wu, *Front. Mater. Sci.*, 2017, 11, p 139.
41. C.M. Magdalane, K. Kaviyarasu, J.J. Vijaya, B. Siddhardha, B. Jeyaraj, J. Kennedy, and M. Maaza, *J. Alloys Compd.*, 2017, 727, p 1324.
42. Y. Yuan, G.-F. Huang, W.-Y. Hu, D.-N. Xiong, B.-X. Zhou, S. Chang, and W.-Q. Huang, *J. Phys. Chem. Solids*, 2017, 106, p 1.
43. L. Zi-ya, Z. Man-ying, and W. Jing-ling, *ChemistrySelect*, 2018, 3, p 10630.
44. H. Wei, L. Wang, Z. Li, S. Ni, and Q. Zhao, *Nano Micro Lett.*, 2014, 3, p 6.
45. S. Rajendran, M.M. Khan, F. Gracia, J. Qin, V.K. Gupta, and S. Arumainathan, *Sci. Rep.*, 2016, 6, p 31641.
46. A. Hamrouni, H. Lachheb, and A. Houas, *Mater. Sci. Eng. B*, 2013, 178, p 1371.
47. Q.-P. Luo, X.-Y. Yu, B.-X. Lei, H.-Y. Chen, D.-B. Kuang, and C.-Y. Su, *J. Phys. Chem. C*, 2012, 116, p 8111.
48. G. Yang, Z. Yan, and T. Xiao, *Appl. Surf. Sci.*, 2012, 258, p 8704.
49. W. Ben Soltan, M.S. Lassoued, S. Ammar, and T. Toupance, *J. Mater. Sci. Mater. Electron.*, 2017, 28, p 15826.
50. D. Cardillo, M. Weiss, M. Tehei, T. Devers, A. Rosenfeld, and K. Konstantinov, *RSC Adv.*, 2016, 6, p 65397.
51. L. Zhu, H. Li, Z. Liu, P. Xia, Y. Xie, and D. Xiong, *J. Phys. Chem. C*, 2018, 122, p 9531.
52. X. Hao, Z. Jin, H. Yang, G. Lu, and Y. Bi, *Appl. Catal. B*, 2017, 210, p 45.
53. J. Deng, L. Chang, P. Wang, E. Zhang, J. Ma, and T. Wang, *Cryst. Res. Technol.*, 2012, 47, p 1004.
54. A.D. Liyanage, S.D. Perera, K. Tan, Y. Chabal, and K.J. Balkus, *ACS Catal.*, 2014, 4, p 577.
55. U.M. García-Pérez, A. Martínez-de la Cruz, and J. Peral, *Electrochim. Acta*, 2012, 81, p 227.
56. S. Phanichphant, A. Nakaruk, and D. Channei, *Appl. Surf. Sci.*, 2016, 387, p 214.
57. D. Channei, B. Inceesungvorn, N. Wetchakun, S. Ukritnukun, A. Nattestad, J. Chen, and S. Phanichphant, *Sci. Rep.*, 2015, 4, p 5757.
58. M. Sridharan, P. Kamaraj, Y.S. Huh, S. Devikala, M. Arthanareeswari, J.A. Selvi, and E. Sundaravadivel, *Catal. Sci. Technol.*, 2019, 9, p 3686.
59. H. Zhang, W. Tian, Y. Li, H. Sun, M.O. Tadé, and S. Wang, *J. Mater. Chem. A*, 2018, 6, p 6265.
60. R.F. Landis, A. Gupta, Y.W. Lee, L.S. Wang, B. Golba, B. Couillaud, R. Ridolfo, R. Das, and V.M. Rotello, *ACS Nano*, 2017, 11, p 946.
61. S. Cheeseman, A.J. Christofferson, R. Kariuki, D. Cozzolino, T. Daeneke, R.J. Crawford, V.K. Truong, J. Chapman, and A. Elbourne, *Adv. Sci.*, 2020, 7, p 1902913.
62. C.M. Magdalane, K. Kaviyarasu, J.J. Vijaya, B. Siddhardha, and B. Jeyaraj, *J. Photochem. Photobiol. B*, 2016, 163, p 77.
63. X. Li, S.M. Robinson, A. Gupta, K. Saha, Z. Jiang, D.F. Moyano, A. Sahar, M.A. Riley, and V.M. Rotello, *ACS Nano*, 2014, 8, p 10682.
64. A. Elbourne, S. Cheeseman, P. Atkin, N.P. Truong, N. Syed, A. Zavabeti, M. Mohiuddin, D. Esrafilzadeh, D. Cozzolino, C.F. McConville, M.D. Dickey, R.J. Crawford, K. Kalantar-Zadeh, J. Chapman, T. Daeneke, and V.K. Truong, *ACS Nano*, 2020, 14, p 802.
65. H.B. Gasmalla, X. Lu, M.I. Shinger, L. Ni, A.N. Chishti, and G. Diao, *J. Nanobiotechnol.*, 2019, 17, p 58.
66. J.M.V. Makabenta, A. Nabawy, C.H. Li, S. Schmidt-Malan, R. Patel, and V.M. Rotello, *Nat. Rev. Microbiol.* 2021, 19, p 23.
67. I.M. Sundaram, S. Kalimuthu, and G. Ponniah, *Compos. Commun.*, 2017, 5, p 64.